Regular Article

The tension of framed membranes from computer simulations

Daniel Hamkens, Claus Jeppesen, and John H. Ipsen[a]

MEMPHYS - Center for Biomembrane Physics, Department of Physics, Chemistry and Pharmacy, University of Southern Denmark, Campusvej 55, DK-5230 Odense M, Denmark

Abstract. We have analyzed the behavior of a randomly triangulated, self-avoiding surface model of a flexible, fluid membrane subject to a circular boundary by Wang-Landau Monte Carlo computer simulation techniques. The dependence of the canonical free energy and frame tension on the frame area is obtained for flexible membranes. It is shown that for low bending rigidities the framed membrane is only stable above a threshold tension, suggesting a discontinuous transition from the collapsed (branched polymer) state to a finite tension extended state. In a tension range above this threshold tension the membranes display power-law characteristics for the equation of state, while higher tension levels includes both an extended linear (elastic) as well as a highly non-linear stretching regime. For semi-flexible membranes a transition from extended to buckled conformations takes place at negative frame tensions. Our analysis indicates that at zero frame tension the crumpling transition of fluid membranes show characteristics of both critical behavior and a discontinuous transition at low bending rigidities.

1 Introduction

The characterization of the physical properties of flexible sheets and membranes remains a challenging research topic. In particular the behavior of self-avoiding tethered (or polymerized) surfaces with fixed in-plane connectivity has been explored by theoretical analysis and computer simulations, where much of the methodology from polymer physics and 2D lattice model systems can be generalized. For the description of the conformations of self-avoiding, flexible, fluid membranes this generalization is less obvious, since the varying connectivity coupled to surface geometry gives rise to a significantly larger phase space. The theoretical analyses of self-avoiding fluid surfaces are mostly based on computer simulations of lattice plaquette models [1, 2] and randomly triangulated surfaces [3, 4]. We find the latter techniques particularly promising, because they allow for formulations of discretized models of surfaces with a trivial continuum limit which can be related to the standard continuum interfacial free energy models. The research in randomly triangulated surface models has mostly focused on the analysis of simple closed membranes with very few surface features, *e.g.*, the bending elasticity or osmotic pressure difference between the interior and the surroundings. For such membranes it has been well established that the free-standing flexible membrane looses its surface character and behaves like a branched polymer comprised of mem-

brane tubes at diameters at the microscopic cut-off length scale l [3–5]. For semi-flexible membranes this picture remains, except for length scales smaller than the persistence length $\xi_P(\kappa) \simeq l \exp(\frac{4\pi\kappa}{3k_BT})$ [6–8], where the membrane appears as rigid with strong correlations between surface normals. κ is the bending rigidity, the elastic constant stabilizing the mean-curvature of the membrane. By increasing the bending rigidity we can thus in a continuous manner reestablish the surface smoothness over distances below $\xi_P(\kappa)$. In contrast to this, it was discovered that the application of a small inflating pressure to a closed, flexible vesicle gives rise to an abrupt *deflation-inflation* transition at a well-defined pressure, to a new phase with interesting new scaling properties [9, 10]. The new vesicle structure then smoothly transforms into the spherical configuration by further increase of the pressure. The properties of the new inflated phase has been interpreted in terms of a generalized model for stretched polymers. However, this interpretation involves several assumptions, *e.g.*, that the osmotic pressure has a simple translation to a surface frame tension in this regime and the absence of a zero-tension limit for a framed membrane. In this study, we have formulated the triangulated surface model with a boundary fixed to a circular frame, which may be controlled by a lateral frame tension to illuminate the properties of flexible membranes at low κ values. This is a direct analogy to the classical linear polymer analysis, where the polymer arc length and the end-to-end distance are the control parameters, the latter possibly

---
[a] e-mail: `ipsen@memphys.sdu.dk`

controlled by a tensile force. By far most of the theoretical literature on fluid membrane conformations is based on descriptions of framed membranes, where fluctuations around a mean shape are analyzed, *e.g.*, the Monge or quasi-spherical representations of membrane shapes. As examples can be mentioned the interesting discussions about the relationship between the various membrane tension definitions [11–16], the interpretation of results from aspiration of vesicles by micro-pipette techniques [17, 18] or optical tweezer [19], and steric repulsive interactions of lamellar membranes [20]. The effect of membrane tension is also of direct consequence for the membrane conformations in biological membranes. The volume of the cytosol and the lumen of the organelles are highly regulated by the osmolarity and thereby this give rise to a lateral tension in the membranes. Furthermore, the biomembranes interact with cyto-skeletal components, thereby modulating the membrane tension. In this work we study the properties of hyper-flexible framed membranes by application of a variant of the Monte Carlo technique, the Wang-Landau method [21], on a self-avoiding triangulated random surface model on a frame. The Wang-Landau technique allows us to give numerical estimates of the free energy under various system conditions. Although the Wang-Landau technique is still under development, it has been applied successfully for a range of problems, *e.g.*, discrete lattice models [21], polymer properties [22], protein conformations [23] and the calculation of reaction rates [24]. In context of triangulated surfaces Wang-Landau algorithms have been used to obtain the genus-dependence of the density of states [25] and the specific heat of fixed connectivity surfaces [26]. This paper is organized as follows: In sect. 2 the framed model is introduced with emphasis on the discretization on the randomly triangulated surface; sect. 3 describes the Monte Carlo simulation technique by Wang and Landau applied to the framed model membrane; sect. 4 gives a brief introduction to the thermodynamics of the framed fluid surface necessary for the interpretation given in the results and discussion sect. 5, and sect. 6 is for conclusions.

2 Model

2.1 Continuum model

The fluid membrane can, to a good approximation, be modeled as a mathematical surface. So, we consider a surface of area A in $\mathcal{R}^3$ which is homeomorphic to a disc. For convenience we chose the boundary of the surface as circular, enclosing an area A_B. Most theoretical descriptions of the conformations of fluid membranes take their beginning in Helfrich's interfacial free energy expression, which in its simplest form becomes [27–29]:

$$\mathcal{H} = \kappa \int (2H)^2 \, \mathrm{d}A + \kappa_G \int_A G \, \mathrm{d}A, \qquad (1)$$

where H is the local mean curvature of the membrane and A is the surface area. The elastic constant κ, the bending
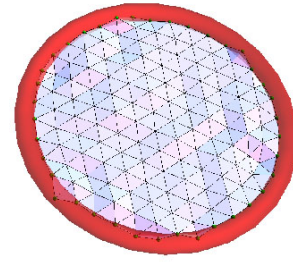
Fig. 1. The frame-based configuration with the confining torus shown in red. The beads are not shown here in order to better visualize the network structure.

rigidity, is an experimentally measurable quantity typically found in the range of 10–50 in units of $k_B T$ for synthetic bilayer membranes. The general Helfrich model also involves a term linear in H, which we abolished since our membrane is featureless and posses up-down symmetry. The last term in eq. (1) involves a term proportional to the Gauss curvature G integrated over the surface, which we neglect here ($\kappa_G = 0$) despite it has an explicit dependence on the boundary. According to Gauss-Bonnett's theorem:

$$\int_A G \, \mathrm{d}A = 2\pi\chi - \oint_{\partial A} \lambda_g \mathrm{d}s, \qquad (2)$$

where the Euler characteristic $\chi = 1$ for a compact disc and λ_g is the geodesic curvature of the boundary curve. Although, we have chosen $\kappa_G = 0$, an effective term of this type may well be generated by simulation of the discretized model [7] or from renormalization effects [6]. However, the contribution eq. (2) is a non-extensive boundary term and is expected to be insignificant for the overall properties of the framed surfaces with fixed topology. For a membrane patch with fixed number of components the total surface area is limited by an additional elastic contribution $\frac{K_A A_0}{2}(\frac{A-A_0}{A_0})^2$ to the free energy, where K_A is the compressibility modulus and A_0 is the equilibrium area. This term becomes dominating when the membrane is subject to high external tension [18].

2.2 Discretization

Any closed surface can be approximated by dividing it into sufficiently many small triangular simplices. Such a triangulated surface consists of a union of triangles, where the corners of the triangles form a set of vertices $\{i\}$ at positions $\mathbf{x}_i$ and the sides of the triangles are referred to as links between vertices. See fig. 1 for an illustration of a triangularized surface patch. The N vertices, $N_T = 2N - N_B - 2$ triangles and $N_L = 3N - N_B - 3$ links together form a planar triangular network bounded by N_B boundary links. The surface triangulation provides an effective method of characterizing surface properties from the discretzed surface. To ensure the fluid character of the surface we need to take into account all possible triangulizations of the surface.

This is handled by random triangulization, where the planar triangular network can change its connectivity.

Randomly triangulated surfaces have been used in investigations of both high energy physics [30–32] and in the description of in-plane fluid phase separation [33] and conformations of simple, fluid membranes (reviewed by Gompper in [34]) and more recently in the description of nematic membranes [35].

2.3 Self-avoidance

To give a realistic description of the large scale conformations of a fluid lipid membrane, the model needs to be self-avoiding. It is a challenging requirement, since the Wang-Landau simulation technique (sect. 3) will explore any corner of the phase space. The specific model used here is a simple bead-and-tether model, where each vertex is at the center of a hard shell with radius σ_0 and the links between the vertices in a triangle have a maximum tether length of l_0. The model is thus a generalization of the pearl necklace model of polymer physics. Such models can both provide self-avoidance of the surface and restrict the surface area to a narrow range.

A simple analysis shows that $\frac{l_0}{\sigma_0} < \sqrt{3}$ is a necessary criterion to maintain a weak self-avoidance condition which has proven practical in MC simulations of rigid membranes [7], but for the general self-avoiding surface problem it is not sufficient [8]. However, the algorithms have shown to become very inefficient as $\frac{l_0}{\sigma_0}$ is reduced. In this work we have chosen to follow another route to maintain full self-avoidance. For convenience we set $\sigma_0 = 1$ and $l_0 = \sqrt{3}$ and implement the constraint that the angle between the normals of any neighboring triangle must not exceed $\frac{2}{3}\pi$. Further conditions to ensure self-avoidance are implemented by making sure that no links intersect with any triangle by maintaining a linked list cell structure, which keeps track of vertex positions, and triangle centroids in any spatial neighborhood. This data structure allows, in conjunction with the triangulization, an efficient selection of potential link-triangle intersections to be examined explicitly for intersections. This procedure is particularly important at the boundary where the above conditions do not apply.

2.4 Discretized model

For numerical analysis the Helfrich free energy expression eq. (1) needs to be discretized, i.e. formulated for the general triangular lattice introduced in the previous section. As a starting point we establish the mean curvature vector in a single vertex constructed from the geometry of its neighborhood. It can been shown that

$$\mathbf{H}(\mathbf{x}_i) = \frac{1}{2A_{i,mixed}} \sum_{j \in N_1(i)} \cot s_{ij} (\mathbf{x}_i - \mathbf{x}_j) \qquad (3)$$

provides a consistent definition of the discretized mean curvature vector [36]. For the link between i and j, $\cot s_{ij}$

is calculated as [37]

$$\cot s_{ij} = \begin{cases} \frac{1}{2}(\cot(\theta_k) + \cot(\theta_l)), & \text{for interior links,} \\ \frac{1}{2}\cot(\theta_k), & \text{for boundary links.} \end{cases}$$

For two neighboring triangles (ijk) and (ijl) of the triangulation θ_k and θ_l are the angles opposite to the side (ij). $N_1(i)$ represents the nearest-neighbor vertices of i. The area $A_{i,mixed}$ is a local area assigned to the Voronoi cell around the vertex i. In case all the triangles of the Voronoi area are non-obtuse, $A_{i,mixed}$ is identical to the standard Voronoi expression

$$A_{i,Voronoi} = \frac{1}{4} \sum_{j \in N_1(i)} \cot s_{ij} \|\mathbf{x}_i - \mathbf{x}_j\|^2. \qquad (4)$$

This area has a simple geometric interpretation based on the circumcenters of the triangles constituting the Voronoi cell. In the case of an obtuse triangle the area contribution from a triangle is chosen as the total area $A_\triangle$ of the triangle. The area of the triangle is divided into 3 pieces, one half the area and two a quarter each. If the obtuse angle is at the vertex i the area contribution is $\frac{A_\triangle}{4}$ and if it is one of the two remaining angles the contribution is $\frac{A_\triangle}{2}$. This procedure ensures that each patch of the entire area of the surface is used one and only once. The above can be formalized as [37]:

$$A_{mixed} = \begin{cases} A_{Voronoi}, & \text{if } T \text{ is non-obtuse,} \\ A_\triangle/2, & \text{if } T \text{ is obtuse at } i, \\ A_\triangle/4, & \text{if } T \text{ is obtuse at } j \text{ or } k. \end{cases}$$

The mean-curvature vector $\mathbf{H}(\mathbf{x}_i)$ gives the magnitude of the mean curvature and the orientation of the surface normal, since $\mathbf{H}(\mathbf{x}) = H\mathbf{n}(\mathbf{x})$, while the direction of the surface normal and sign of the mean curvature has to be determined independently. Therefore an estimate of the normal $\mathbf{n}_v(\mathbf{x})$ at a vertex is calculated by averaging the normals of the surrounding triangles weighted by their A_{mixed} contribution. This gives the final equation for the mean curvature squared of the entire surface:

$$\int \mathrm{d}A H^2 = \sum_{i \in vertex} A_{i,mixed} (\mathbf{H}(\mathbf{x}_i) \cdot \mathbf{n}_v(\mathbf{x}_i))^2. \qquad (5)$$

Equation (5) will be used throughout the simulations.

3 Wang-Landau simulation

3.1 The principles of the Wang-Landau simulation

The Wang-Landau method takes it beginning in Lee's entropic sampling scheme [38]. Let us consider the partition

function over the micro-states η for the discretized membrane with N vertices and $\kappa = 0$:

$$Z_N(T,\tau) = \sum_\eta \exp\left(-\beta\tau A(\eta)\right)$$
$$= \int dA_B \, g_N(A_B) \exp\left(-\beta\tau A_B\right), \qquad (6)$$

where $A_B(\eta)$ is the framed area for the micro-state, $g_N(A_B) = \sum_\eta \delta(A_B(\eta) - A_B)$ is the density of states and $\beta = 1/k_B T$. The corresponding Metropolis importance sampling transition probability between micro-states η and η' is given by

$$p_{\eta\eta'} = \min\left\{1, \exp\left(-\beta\tau(A_B(\eta) - A_B(\eta'))\right)\right\}. \qquad (7)$$

The probability of finding the membrane with a particular frame area A_B fulfills

$$P_N(A_B) \propto \exp(S_N(A_B)/k_B - \beta\tau A_B), \qquad (8)$$

where $S_N(A_B) = k_B \ln(g_N(A_B))$ is the micro-canonical entropy. Following Lee [38] we can instead choose to sample the system to generate the distribution

$$P_N(A_B) \propto \exp(S_N(A_B)/k_B - \Phi(A_B)) \qquad (9)$$

with the corresponding Metropolis transition probabilities between micro-states:

$$p_{\eta\eta'} = \min\left\{1, \exp\left(-\left(\Phi(A_B(\eta)) - \Phi(A_B(\eta'))\right)\right)\right\}. \qquad (10)$$

If $\Phi(A_B)$ is chosen so $P_N(A_B) = $ const, or equivalently $S_N(A_B)/k_B - \Phi(A_B) = $ const, the simulation scheme has generated a procedure to calculate the entropy function numerically up to a constant. Based on these considerations Wang and Landau [21] devised an effective, iterative method to numerically obtain an approximate entropy function (or $\Phi(A_B)$). For the framed membrane, it is implemented by first dividing the area range into M bins. These bins serve as the foundation for two histograms, one for the density of states $g(A_B)$ and one where the number of times a particular bin has been visited in this iteration $H(A_B)$.

The iterations start with a completely flat $\Phi(A_B) = $ const or a $\Phi(A_B)$ obtained from an earlier simulation. After a trial move is either accepted or rejected according to the transition probability eq. (10), the current bin i is updated with a positive modification factor f in the Φ-histogram as $\Phi(A_B^{(i)}) = \Phi(A_B^{(i)}) + f$ and the histogram over visited states is updated as $H(A_B^{(i)}) = H(A_B^{(i)}) + 1$. This strongly penalizes the already-visited states, since a new visit is more likely to be rejected by the Metropolis algorithm. The new $\Phi(A_B^{(i)})$ is likely a better estimate of the entropy function than the old. This form the basis for an iterative scheme which will produce a series of estimates of $\Phi(A_B)$ converging toward the entropy function. If the Φ-histogram is an accurate estimate of $S(A_B)/k_B$, the frequency of the visited states $H(A_B)$ will be the same. However, since the Φ-histogram is just an approximation and

the simulations are finite, the $H(A_B)$-histogram is only approximately flat. As a criterion for flatness we choose that no bin should have more than $\pm 10\%$ of the mean value of the H. When $H(A_B)$ is *flat* the modification factor f is reduced after each iteration by $f_{i+1} = \frac{f_i}{1.75}$. $H(A_B)$ is then set to zero and a new iteration starts. This is done until f becomes small ($f < 10^{-10}$). Unfortunately, the simulation dynamics is non-Markovian by this procedure, since the transition probabilities become simulation time dependent. However, as f gets smaller the modifications of Φ diminishes and the simulation dynamics becomes asymptotically Markovian, as the changes in the transition probabilities become negligible.

3.2 Mixed ensemble simulation by WL

For $\kappa \neq 0$ the above considerations are not sufficient for the description of the thermodynamics of a framed membrane. The entropic sampling can be generalized to the calculation of entropy of any set of extensive variables, or a combination of extensive and intensive variables, which we called mixed sampling. For the control variables τ and A_B this is easily seen by rewriting the partition function

$$Z_N(T,\tau) = \sum_\eta e^{-\beta E(\eta) - \beta\tau A_B(\eta)}$$
$$= \sum_{A_B} \left(\sum_\eta \exp(-\beta E(\eta))\delta\left(A_B - A_B(\eta)\right)\right) \exp(-\beta\tau A_B)$$
$$= \sum_{A_B} g_N(A_B, T) \exp(-\beta\tau A_B). \qquad (11)$$

In this work $E(\eta)$ is the energy of the surface (eq. (1) with the approximation eq. (3)) for the micro-state η representing a configuration of the discretized surface. The considerations of sect. 3.1 can now be applied to this case with the modification that the canonical entropy $S_N(A_B, T) = k_B \ln(g_N(A_B, T))$ is calculated and the simulations must be devised so that $S_N(A_B, T)/k_B - \beta E - \Phi(A_B, T) = $ const. This is ensured with the following transition probability between micro-states:

$$p_{\eta,\eta'} = \min\left\{1, e^{-\beta(E(\eta') - E(\eta)) - (\Phi(A_B(\eta')) - \Phi(A_B(\eta)))}\right\}. \qquad (12)$$

Otherwise, the recipe given in sect. 3.1 is followed.

3.3 Move classes

The generation of valid states for the Monte Carlo procedure is performed by a series of incremental changes of states, so-called moves. The moves of the randomly triangulated framed surface fall into five move classes.
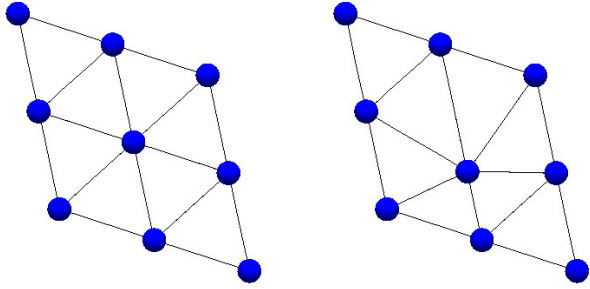
3.3.1 Linkflip

The fluidity of the membrane is maintained by changes in the vertex connectivity of the triangulization network. To
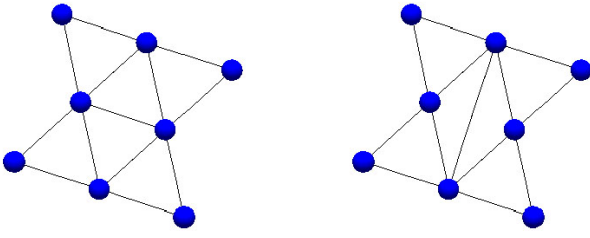
Fig. 2. A linkflip with most of the surrounding network not shown.

Fig. 3. The movement of a single vertex changes the triangles around it.

change the vertex connectivity of the network, the links can be *flipped*. Each link is a side of two triangles. This link can then be flipped so the two previously unconnected vertices in the two triangles are connected (see fig. 2). To maintain the topology of the surface, such a move can only take place, if the originally connected vertices have more than three links and the two new vertices are not connected prior to the flip. Also, self-avoidance must be maintained in the linkflip. Links between boundary vertices cannot be flipped.

3.3.2 Vertex move

The second move class is the vertex move, where a single vertex undergoes a translation (see fig. 3). A vertex is allowed to undergo a small displacement within a ball of radius d in space. This displacement is possible, if there is no overlap between two beads or the tether restrictions are violated, *i.e.* the distance between any vertices i and j fulfill $dist(i,j) > 1$ and $dist(i,j) < \sqrt{3}$ for nearest-neighbor vertices. In general the displacement must not violate the self-avoidance condition, see sect. 2.3. An initial value $d = 0.1$ is chosen for each simulation and then a short calibration run is made to find a d-value where the acceptance ratio is around 0.5. Boundary vertices must be confined to the boundary torus.

3.3.3 Inner-to-boundary vertex conversion

The boundary radius is varying during the simulation, so the exchange of vertices between the boundary and the interior of the surfaces must be conducted. For an inner

vertex to be converted to a boundary vertex several constraints have to be fulfilled: the vertex must have two neighbors which are boundary vertices and be situated between those inside the boundary torus. If the vertex is connected to more than two pairs of boundary vertices, one pair is chosen at random for the vertex to be placed in between. The generation of suitable trial moves of this type is rather low in the Monte Carlo procedure.

3.3.4 Boundary-to-inner vertex conversion

For a boundary vertex to become an inner vertex the following has to be satisfied: the total number of boundary vertices cannot be lower than 6. This is introduced to satisfy that the boundary approximately follow the major circle of the boundary torus. To make sure that the ring of boundary vertices only surrounds one section of inner vertices, the chosen vertex has to be connected to at least one inner vertex. If a conversion takes place, then a new triangle is formed, which has to satisfy the previously described requirements of triangles in sect. 3.3.1. Similarly, the newly formed link must fulfill the conditions described in sect. 2.3.

3.3.5 Frame re-size

A frame re-size trial move is performed for every N trial moves. When generating a new frame with radius $r_{old} + d$, all boundary vertices has to lie inside the new frame. The frame is also allowed to move a small amount in the (x, y)-plane.

3.4 Detailed balance for boundary conversions

For both boundary move classes in sect. 3.3.3 and sect. 3.3.4 a boundary vertex is picked. For the inner-to-boundary conversion, an inner vertex connected to, at least, one boundary vertex is chosen to improve the chance of the vertex to be a valid candidate for conversion, since it is within or near the torus. For detailed balance to be obeyed, it should be equally probable to select the transitions $\eta \to \eta'$ and $\eta' \to \eta$. In the method chosen here, the probability of choosing a specific move depends on the number of boundary links in the configuration, which is not constant. The transition probability must obey the detailed balance condition

$$\frac{\alpha}{n_{\text{boundarylinks}}} = \frac{\beta}{n_{\text{boundarylinks}+1}}, \qquad (13)$$

where α and β are the acceptance probabilities for the move classes in sect. 3.3.3 and sect. 3.3.4. In eq. (13) going from left to right is a boundary-to-inner conversion and going from right to left is an inner-to-boundary conversion.

4 Thermodynamics of framed, fluid surfaces

The outcome from the Wang-Landau Monte Carlo simulation is a density of states $g_N(T, A_B)$, which contains information about the thermodynamic properties of the framed membrane system. This information can either be extracted from the derivatives of the Helmholtz free energy $F(T, A_B, N) = -k_B T \ln(g_N(T, A_B))$ or from averages of the probability distribution $P_{N,T}(A_B) = \frac{g_N(T, A_B)}{Z_N(T)}$, where $Z_N(T) = \int dA_B g_N(T, A_B)$. We will first establish a framework for the discussion of the properties of the framed, fluid surface in the thermodynamic limit (N large), and then explore the possible scenarios for the free energy and establish some nomenclature.

4.1 The thermodynamic limit

The internal energy U of the framed membrane fulfills the fundamental thermodynamic form

$$dU = T\,dS + \tau\,dA_B + \mu\,dN \tag{14}$$

or equivalently in the Helmholtz representation (T, A_B, N) it becomes $dF(T, A_B, N) = -S\,dT + \tau\,dA_B + \mu\,dN$. Therefore, we can characterize the behavior of the membrane by the specific free energy

$$f(T, a_B) = \frac{F(T, A_B, N)}{N} = \mu + \tau a_B, \tag{15}$$

where $a_B = \frac{A_B}{N}$. T is constant in the following considerations and will be omitted in the notation. A necessary condition for mechanical equilibrium at fixed tension τ is thus

$$\tau = \frac{\partial f}{\partial a_B} \tag{16}$$

with the stability criteria $\frac{\partial^2 f}{\partial a_B^2} = \frac{\partial \tau}{\partial a_B} \geq 0$.

Everywhere convex $f(a_B)$

In [39] David and Leibler discussed some basic properties of $f(a_B)$ when it is everywhere convex. Two basic senarios are possible:

1-i) $f(a_B)$ has a minimum at some finite a_B^0, $0 < a_B^0 < a_B^{\max}$, which corresponds to an overall *flat* state $A_B \propto N$ of a tension-less membrane. For non-vanishing tensions a_B will be vary smoothly according to eq. (16).

2-i) Here $f(a_B)$ has its minimum at $a_B = 0$, a *crumpled* state. The corresponding tension τ^0 will in general be non-vanishing, $\tau^0 > 0$, and a continuous *crumpling* of the membrane takes place for $\tau \to \tau^{0+}$. For tensions below τ^0 no a_B can be assigned the membrane and a discontinuous change to a *collapsed* state is expected, *e.g.*, branched polymer configurations.
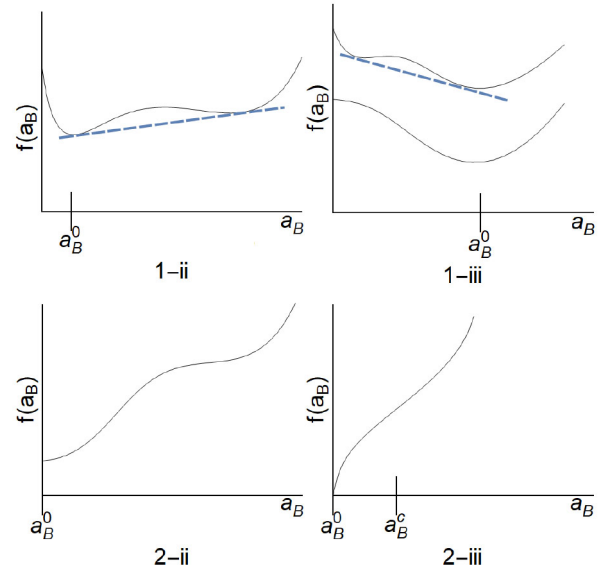
Fig. 4. Sketches of some of the non-convex cases of $f(a_B)$ discussed in sect. 4.1. 1-ii) The slope of the common tangent is equal to the positive transition tension between two *flat* states. 1-iii) The slope of the common tangent is the negative transition tension between two *flat* states. For the lower $f(a_B)$ shown the membrane collapse at a negative tension. 2-iii) a_B^c mark the inflection point of $f(a_B)$.

Convex $f(a_B)$ except for a concave interval

In the following we will extend these considerations to the case where $f(a_B)$ has a concave region in $0 \leq a_B < a_B^{\max}$. Some of the possibilities are illustrated in fig. 4. When $f(a_B)$ has a minimum at a_B^0, $0 < a_B^0 < a_B^{\max}$, there will be a tension-free, *flat* equilibrium state of the membrane as described above.
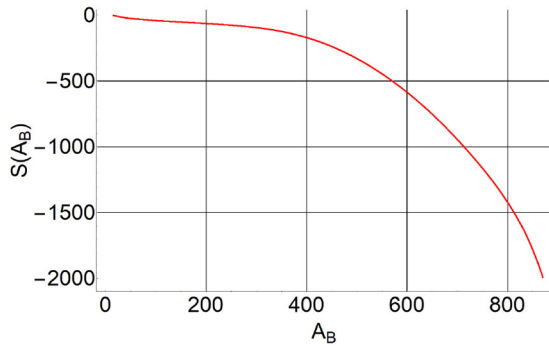
1-ii) If the concave region is above a_B^0 a discontinuous transition between two *flat* states takes place at some tension $\tau \geq 0$, both obeying eq. (16) (see fig. 4).

1-iii) For a concave domain of $f(a_B)$ below a_B^0, a discontinuous transition at a negative tension takes place, either between two *flat* states as above, or a *flat* and *collapsed* membrane when $\frac{\partial^2 f}{\partial a_B^2} < 0$ at $a_B = 0$ (see fig. 4).
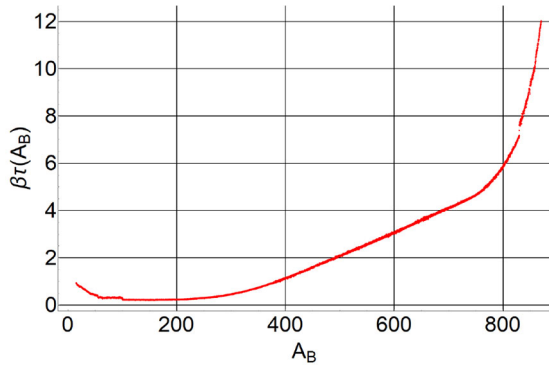
When the minimum of $f(a_B)$ is located at the lower boundary, $a_B^0 = 0$, with the slope $\tau^0 \geq 0$ there will be two possibilities:

2-ii) $\frac{\partial^2 f}{\partial a_B^2} > 0$ at $a_B = 0$, a transition between two flat states take place at $\tau > \tau^0$ (see fig. 4) or between a flat phase and the crumpled phase at $\tau = \tau^0$. At tensions below τ^0 the membrane is in a collapsed state.

2-iii) For $\frac{\partial^2 f}{\partial a_B^2} < 0$ at $a_B = 0$ the framed membrane is undefined, *i.e.* collapsed, in the region $0 < a_B < a_B^c$, where $\frac{\partial^2 f}{\partial a_B^2} = 0$ at a_B^c (see fig. 4). A framed membrane can thus be stabilized for $\tau \geq \tau^c = \frac{\partial f}{\partial a_B}(a_B^c)$. At τ^c a discontinuous

Fig. 5. Entropy $S(T, A_B)$ *versus* projected area A_B for $\kappa = 0$ and $N = 400$.

Fig. 6. The frame tension $\beta\tau$ *versus* A_B for $N = 400$ and $\kappa = 0$. $\beta\tau$ is derived from $S(T, A_B)$ shown in fig. 5. Note that the frame tension stays positive everywhere.
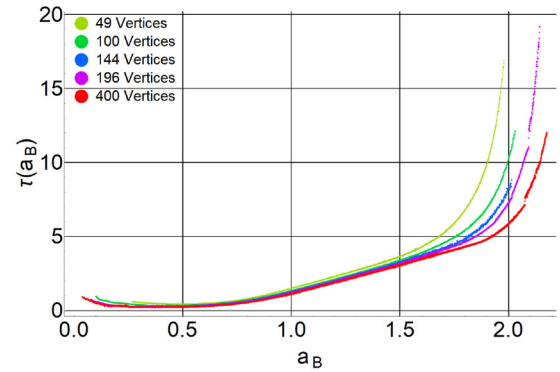

Fig. 7. The effect of the system size on the membrane stretching at $\kappa = 0$. $\beta\tau$ versus a_B displays a noticeable N-dependence in the strectching regime, while the effect of the system size can hardly be resolved at low a_B values. The tension is positive in the whole a_B range.

$\beta\tau$ is plotted against A_B. The shown case is for $N = 400$ and $\kappa = 0$. Such curves make it possible to conduct an analysis along the lines described in sects. 3.2 and 4. The stretching curves are robust over a wide range of frame areas, while the convergence of the Wang-Landau procedure becomes very slow in ranges close to the minimal and maximal possible areas. The quality of the free energy determination and the estimation of the tension is thus hampered close to these boundaries and long simulation times are required. Also, for increasing values of κ the convergence of this Wang-Landau algorithm becomes very slow. It has therefore only been possible to analyze the system for small κ values less than $3k_BT$.

5.2 Floppy membranes, $\kappa = 0$

In fig. 7 are shown stretching curves for the membrane ($\beta\tau$ *vs.* a_B) for $N = 49, 100, 144, 196$ and 400. The figure shows that the overall shape of the stretching curves is the same for most of the stretching region for the system sizes considered. A striking observation is the absence of a thermodynamically stable frame tension-free state, since the lowest tension τ_c is positive for all the observed system sizes. This minimum in $\tau(a_B)$ occurs for some $a_B = a_B^c > 0$ with

$$\frac{\partial\tau}{\partial a_B} = 0, \tag{17}$$

indicating a region $a_B < a_B^c$, where $\frac{\partial\tau}{\partial a_B} < 0$ and the framed membrane is thermodynamically unstable. Since $\tau(a_B)$ keeps rising for $a_B \to 0^+$, it suggests that the whole region $0 < a_B < a_B^c$ is unstable. In the discussion in sect. 4 the flexible membrane thus falls into the category 2-iii), where τ_c marks the lower tension limit of the framed membrane model. Beyond this tension, the framed membrane has a discontinuous collapse into a state, which cannot be characterized by a finite framed tension, *e.g.*, the branched polymer configurations. However, τ_c also has the characteristics of a critical point for $\tau \to \tau_c^+$ due to the condition

collapse of the membrane will take place, nevertheless, at tensions close to τ^c it may display a critical behavior with the diverging response function $\frac{\partial a_B}{\partial\tau}$.

The simulation results presented in the next section suggest that both the scenarios 1-iii) and 2-iii) are in play for the flexible and semi-flexible framed membranes. In the above discussion we have not considered the conditions close to maximal specific projected area $a_B^{\max}$, where no configurational or extensional fluctuations can take place. We therefore expect $\tau = \frac{\partial f}{\partial a_B} \to \infty$ for $a_B \to a_B^{\max}$. In this stretching limit a plausible phenomenological form is $f(a_B, T) \simeq f(T, a_B^{\max}) + cst \cdot |a_B^{\max} - a_B|^\omega$, where $0 \le \omega < 1$ with $\omega = 0$ corresponding to the logarithmic dependence.

5 Results and discussion

5.1 The free energy

The results of a simulation can be described by a numerical estimate $\Phi(A_B, T, N)$ of $S(A_B, T, N)/k_B - \beta E = -F(A_B, T, N)\beta$ up to an arbitrary constant. In fig. 5 the dependence of $\Phi(A_B, T, N)$ on A_B is shown. The corresponding tension is obtained from $\Phi(A_B, T, N)$ by use of eq. (11) and eq. (16). This tension is shown in fig. 6, where

Table 1. Data for a_B^c, τ_c, δ, $2\nu'$ obtained from fits in the low tension regime.

N	49	100	144	196	400
a_B^c	0.51(2)	0.35(1)	0.41(1)	0.41(1)	0.41(1)
τ_c	0.38	0.31	0.28	0.25	0.0171
δ	1.70	2.65	2.30	2.36	2.34
$2\nu'$	0.63	0.73	0.70	0.70	0.70

eq. (17) and $\frac{\partial \tau}{\partial a_B} > 0$ for $a_B > a_B^c$. This suggests the non-linear behavior

$$\beta(\tau - \tau_c) \simeq \rho(a_B - a_B^c)^\delta = \rho \left(\frac{A_B - A_B^c}{N} \right)^\delta, \qquad (18)$$

where ρ is a constant, δ is a stretching exponent, and $A_B^c = a_B^c N$. Equation (18) has some similarity with the Pincus stretching regime for a self-avoiding polymer [40]. For τ close to τ_c we can invoke the hyperscaling relation $\beta(\tau - \tau_c)(A_B - A_B^c) \simeq 1$ which leads to the relationship

$$A_B - A_B^c \simeq \rho^{-2\nu'-1} N^{2\nu'}. \qquad (19)$$

Here, we have introduced the exponent ν' with $2\nu' = \frac{\delta}{\delta+1}$, which relates the internal with the external (frame) dimension of the membrane. Averaged over the four largest system sizes (table 1) it is found $2\nu' = 0.71 \pm 0.01$, which gives a clear indication of a non-trivial critical behavior. This value is somewhat lower than the Flory estimate of 0.8 obtained for Gaussian, self-avoiding surfaces [41] or the estimated exponent found in computer simulations of pressurized vesicles above the inflation transition [9,10]. However, our findings are in good accordance with the observed inflation transition pressure $p^* \sim N^{-w}$ where $w \simeq 0.5$ for $\kappa = 0$ for closed vesicles [9]. The transition pressure can readily be obtained from our minimum threshold tension τ_c by use of Laplace law $p^* = \frac{2\tau_c}{R_G}$, where the radius of gyration R_G can be identified with the radius of a spherical frame,

$$p^* = \frac{4\tau_c \sqrt{\pi}}{\sqrt{A_B^c}} = \frac{4\tau_c \sqrt{\pi}}{\sqrt{a_B^c N}} \sim N^{-0.5}. \qquad (20)$$

The inflation transition is accompanied by apparent critical behavior with non-trivial scaling in radius of gyration and volume [9,10]. However, the above results for flexible, framed membranes suggest that in the thermodynamic limit these vesicle size quantifiers posses a trivial scaling behavior, since $R_G^2 \propto A \simeq a_B^c N + \rho^{-2\nu'-1} N^{2\nu'}$ and $V \propto (a_B^c N + \rho^{-2\nu'-1} N^{2\nu'})^{\frac{3}{2}}$. We note that this result is in agreement with the real-space renormalization group analysis of pressurized lattice vesicles [42]. In fig. 7 are shown stretching curves for the flexible membrane for different system sizes and the obtained values of τ_c, a_B^c, δ and ν' are given in table 1.

Beyond this highly non-linear elastic regime we find a range of tensions ($\beta\tau \simeq 1$–5) with approximately linear elastic behavior $\tau = \tau^m + K_A \frac{a_B - a_B^m}{a_B^m}$. (a_B^m, τ^m) marks

Table 2. Fitted values of a_B^m, $\beta\tau^m$ and βK from the linear stretching regime.

N	49	100	144	196	400
$\beta \frac{\partial \tau}{\partial a_B}$	4.24(1)	4.22(8)	4.29(3)	4.00(0)	3.96(3)
a_B^m	1.16	1.20	1.19	1.22	1.21
$\beta\tau^m$	2.15(1)	2.11(5)	2.06(7)	2.08(2)	2.09(3)
βK	4.64	4.75	5.11	5.15	5.13
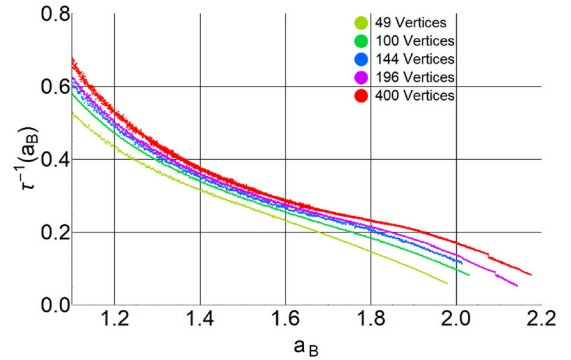
Fig. 8. τ^{-1} *vs.* a_B in the stretching regime for $\kappa = 0$.

the middle of the region with constant $\frac{\partial \tau}{\partial a_B}$ and $K_A = a_B \frac{\partial \tau}{\partial a_B}$ is the corresponding compressibility modulus (see table 2). It is illuminating to compare the averaged value $\beta K_A = 0.023$ with the compressibility modulus of the corresponding planar "Fisherman's net" $\beta K_A = a_B \frac{\partial \beta\tau}{\partial a_B} = \frac{\langle a_B \rangle}{\langle a_B^2 \rangle - \langle a_B \rangle^2} \simeq 1$ [43]. We thus conclude that this linear elasticity regime is much softer than expected from the planar expansion of an entropic net and out-of-plane configurational entropy must play a significant role. At high tension levels, a_B approaches its maximum as illustrated in fig. 8. It is evident that this regime is a property of the discetized model, which is not represented in the continuum description. It is found that even at the highest extensions we can sample, about 90% of the maximal extension, the asymptotic relationship $\beta\tau = \frac{2a_B^{max}}{a_B} \frac{1}{a_B^{max} - a_B}$ [43,44] for a planar "Fisherman's net" is not reached, suggesting that the disclinations and out-of-plane configurations are important.

### 5.3 Semi-flexible membranes, $\kappa \simeq k_B T$

The properties of the hyperflexible membrane $\kappa = 0$ are expected to persist at very low bending rigidities. In this section the transition from a flexible to a rigid membrane behavior is analyzed. In fig. 9 is shown a series of stretching curves for $N = 400$ and different values of κ in a range up to $2k_B T$. For small values of κ ($\beta\kappa \leq 0.5$) the behavior observed is very similar to the $\kappa = 0$ case described in sect. 5.2. We can thus generalize eq. (18) for small κ

$$\tau = \rho(\kappa)|a - a_B^c(\kappa)|^{\delta(\kappa)} + \tau_c(\kappa), \qquad (21)$$
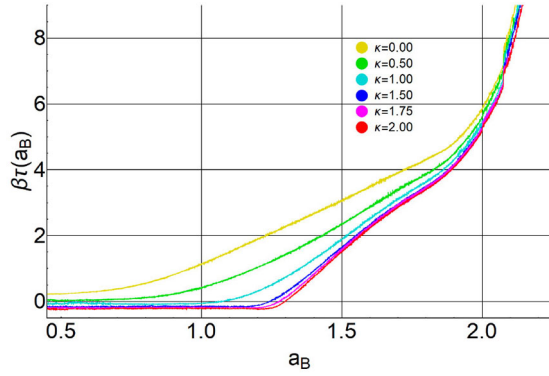
Fig. 9. Tension $\beta\tau(a_B)$ *versus* projected area a_B for $N = 400$ and various values of $\beta\kappa$.
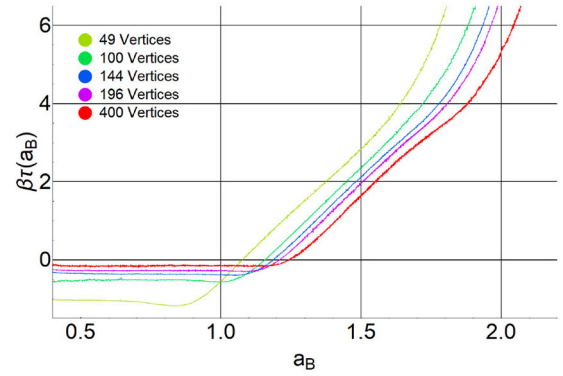
Fig. 10. Tension $\beta\tau(a_B)$ *versus* projected area a_B for various values of N and $\beta\kappa = 1.5$.

Table 3. Fitted values of $\frac{\partial\tau}{\partial a_B}$, a^0 and βK_A at a^0 for varying κ and N.

|	$\beta\frac{\partial\tau}{\partial a_B}$		
$N =$	49	144	196
κ			
0	4.24	4.29	4.00
0.5	4.81	5.24	5.21
1.0	5.77	6.00	6.10
1.5	6.72	6.77	6.73
	a^0		
$N =$	49	144	196
0	1.16	1.19	1.22
0.5	1.22	1.47	1.50
1.0	1.23	1.45	1.49
1.5	1.22	1.44	1.50
	βK_A		
$N =$	49	144	196
0	4.64	5.11	5.15
0.5	5.87	7.70	7.84
1	7.10	8.82	9.01
1.5	8.21	9.82	10.10

where $\rho(\kappa) > 0$, $\tau_c(\kappa)$, $\delta(\kappa)$ and $a_B^c(\kappa)$ are some smooth functions of κ. Here $\rho(\kappa) > 0$, $a_B^c(\kappa)$ is increasing, while the threshold tension $\tau_c(\kappa)$ is decreasing with κ, *i.e.* a collapse of the framed membrane at $\tau_c(\kappa)$ with critical behavior when $\tau \to \tau_c(\kappa)^+$. Unfortunately, it was not possible to determine the exponent $\delta(\kappa)$, since the regime of approximate scaling behavior becomes small. Also, the linear stretching regime diminishes, while the strong stretching regime is closely following the $\kappa = 0$ behavior. For $\kappa = \bar{\kappa}$, with $\beta\bar{\kappa} \simeq 0.6$, we find that the membrane is tension-free at the collapse transition, $\tau_c(\bar{\kappa}) = 0$. For further increase in κ the tension-free state becomes thermodynamically stable and the associated specific area $a_B^0(\kappa)$ is increasing (table 3), while the membrane undergoes a transition

at a negative tension $\tau_r(\kappa)$ from the extended conformation $a_B^r(\kappa)$ to a small specific area, which unfortunately cannot be identified. Furthermore, the signature of critical behavior at tensions close to the transition tension $\tau_r(\kappa)$ disappears, since $\frac{\partial\tau}{\partial a_B} > 0$ and increases at $a_B^r(\kappa)$. In this regime we find approximately $\tau_r(\kappa) \propto -\kappa$. For $\kappa \simeq \bar{\kappa}$ the stretching curves display a strong variation with the system size. This can indicate a cross-over behavior of the system in a parameter range where an intrinsic length scale (the persistence length) and the system size $\sqrt{Nl^2}$ are similar. For small system sizes we find that a tension-free state is stable and $\tau_r(\kappa) < 0$ (see fig. 10). For large system sizes the collapse tension $\tau_r(\kappa)$ is well defined with $0 < \tau_r(\kappa) < \tau_r(0)$.

In fig. 10 is shown the size dependence of the stretching curves for a more rigid framed membrane with $\beta\kappa = 1.5$. Here the collapse transition takes place at negative tension values for the analyzed system sizes. It is interesting to note that we here observe $\tau_r(1.5k_BT) \propto -1/N$ and $a_B^r(1.5k_BT) \propto N$. Therefore, $\tau_r(1.5k_BT) \propto -\kappa/N$ and it is natural to interpret the collapse transition in this regime as a simple buckling of the rigid membrane, subject to negative lateral tension. The observed independence of $\tau(a_B)$ from a_B is consistent with this interpretation. In the classification given in sect. 4 the framed membrane crosses over from the 2-iii) to the 1-iii) behavior above $\bar{\kappa}$.

5.4 Tension-free membranes

The above considerations show that floppy, framed self-avoiding membranes are only stable above some threshold tension $\tau_c(\kappa)$. Also, they show that for $\kappa \geq \bar{\kappa}$, a stable tension-free state exists. This is demonstrated in fig. 11 where $A_B(\tau = 0, \kappa)$ is plotted *versus* κ for $N = 400$. For the tension-free membrane the projected area shows small variations with κ for rigid membranes, while it vanishes as $\kappa \to \bar{\kappa}^+$ in an apparent singular manner. This behavior can be understood from eq. (21). For $\tau_c(\kappa) \simeq 0$ we can linearize $\tau_c(\kappa) \simeq \tau_c'(\bar{\kappa})(\kappa - \bar{\kappa})$ with $\tau_c'(\bar{\kappa}) < 0$ and $a_B^c(\kappa) \simeq a_B^c(\bar{\kappa}) + a_c'(\bar{\kappa})(\kappa - \bar{\kappa})$ with $a_c'(\bar{\kappa}) > 0$. Combining this with eq. (21) we expect that the leading behaviour of a_B for a
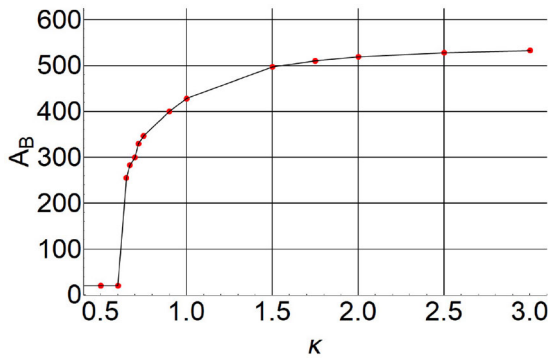
Fig. 11. Projected area $A_B(\tau = 0, \kappa)$ for the tension-free membrane *versus* $\beta\kappa$ for $N = 400$.
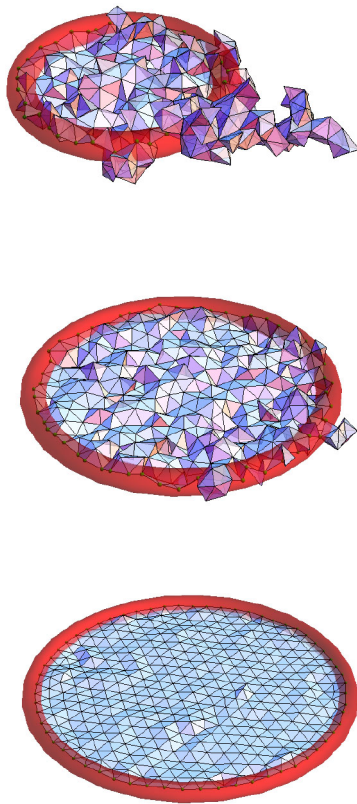
Fig. 12. Configurational snapshots.

tension-free membrane at $\kappa \gtrsim \bar{\kappa}$ is

$$a_B^0(\kappa) = a(\tau = 0, \kappa) \sim |\kappa - \bar{\kappa}|^{\frac{1}{\delta}}, \qquad (22)$$

where $\bar{\delta} = \delta(\bar{\kappa})$. Unfortunately, the accuracy of the data in fig. 11 is not sufficient to estimate an exponent characterizing the singular behavior of $A_B(\tau = 0, \kappa)$ for κ approaching $\bar{\kappa}$. The results of this section confirms that the free-standing (tension-free and unsupported) membrane does not exist below a bending rigidity $\beta\bar{\kappa} \simeq 0.6$. The existence of such a low-κ limit for the stability of membranes was predicted by David and Guitter by large-d analysis of self-intersecting membranes [45, 46]. It is interesting to note that the various discretized models of

rigid, self-avoiding triangulated surfaces all show a cusp in the specific heat of free-standing vesicles at $\beta\kappa$ values close to 1 [7, 8, 35], which coincide with the lower limit of the behavior of membranes expected from the continuum description of rigid membranes [8].

Figure 12 shows configurational snapshots from the Wang-Landau Monte Carlo simulation of the framed membrane model for $\kappa = 0$, $N = 400$ and $a_B = 0.39, 1.06, 2.26$.

6 Conclusion

We have performed a numerical analysis of the free energy and the tension-extension relationship for framed, fluid membranes at low bending rigidities. The membrane was described by a randomly triangulated self-avoiding surface model, which was analyzed by Wang-Landau Monte Carlo computer simulation techniques. The simulation results demonstrated that for flexible membranes there exists a minimal threshold tension τ_c at a non-zero specific frame area a_B^c, below which the framed membrane is mechanically unstable, with an accompanying discontinuous collapse of the surface. Approaching τ_c from above the membrane displays critical behavior with an exponent $\nu' \simeq 0.36$. This behavior is changed by the bending stiffness of the membrane. For bending rigidities above the threshold $\beta\bar{\kappa} \simeq 0.6$, the stable framed membranes prevails for all $\tau \geq 0$. In particular free-standing membranes are only stable for $\kappa \geq \bar{\kappa}$.

Author contribution statement

Daniel Hamkens developed and implemented the code, conducted the Wang-Landau Monte Carlo simulations and data analysis, and wrote the paper. Claus Jeppesen developed the basic Dynamic Triangulated Surface (DTS) code and performed data interpretation. John H. Ipsen developed the basic DTS code, planned the project, conducted data interpretation and wrote the paper.

References

1. U. Glaus, J. Stat. Phys. **50**, 1141 (1988).
2. J. O'Connell, F. Sullivan, D. Libes, E. Orlandini, M.C. Tesi, A.L. Stella, T.L. Einstein, J. Phys. A **24**, 4619 (1991).
3. D.M. Kroll, G. Gompper, Phys. Rev. A **46**, 3119 (1992).

4. C. Jeppesen, J.H. Ipsen, Europhys. Lett. **22**, 713 (1993).
5. B. Durhuus, J. Frölich, T. Jonsson, Nucl. Phys. B **283**, 185 (1983).
6. L. Peliti, S. Leibler, Phys. Rev. Lett. **54**, 1690 (1985).
7. G. Gompper, D.M. Kroll, Phys. Rev. E **51**, 514 (1995).
8. J.H. Ipsen, C. Jeppesen, J. Phys. I **5**, 1563 (1995).
9. G. Gompper, D.M. Kroll, Phys. Rev. A **46**, 7466 (1992).
10. B. Dammann, H.C. Fogedby, J.H. Ipsen, C. Jeppesen, J. Phys. I **4**, 1139 (1994).
11. W. Cai, T.C. Lubensky, P. Nelson, T.R. Powers, J. Phys. II **4**, 931 (1994).
12. O. Farago, P. Pincus, Eur. Phys. J. E **11**, 399 (2003).
13. C. Barbetta, A. Imparato, J.-B. Fournier, Eur. Phys. J. E **31**, 333 (2010).
14. J.-B. Fournier, C. Barbetta, Phys. Rev. **100**, 078103 (2008).
15. H. Shiba, H. Noguchi, J.-B. Fournier, Soft Matter **12**, 2373 (2016).
16. H. Koibuchi, A. Shobukhov, H. Sekino, J. Math. Chem. **54**, 358 (2016).
17. E. Evans, W. Rawicz, Phys. Rev. Lett. **64**, 2094 (1990).
18. J.R. Henriksen, J.H. Ipsen, Eur. Phys. J. E **14**, 149 (2004).
19. J.-B. Fournier, A. Ajdari, L. Peliti, Phys. Rev. Lett. **86**, 4970 (2001).
20. W. Helfrich, Z. Naturforsch. A **33**, 305 (1978).
21. F. Wang, D.P. Landau, Phys. Rev. Lett. **86**, 2050 (2001).
22. P.N. Vorontsov-Velyaminov, N.A. Volkov, A.A. Yurchenko, J. Phys. A: Math. Gen. **37**, 1573 (2004).
23. A.D. Swetnam, M.P. Allen, J. Comput. Chem. **32**, 816 (2011).
24. B. Nielsen, C. Jeppesen, J.H. Ipsen, J. Biol. Phys. **32**, 465 (2006).
25. B. Krüger, K. Mecke, Phys. Rev. D **93**, 085018 (2016).
26. H. Koibuchi, J. Stat. Phys. **140**, 676 (2010).
27. W. Helfrich, Z. Naturforsch. C **28**, 693 (1973).
28. P. Canham, J. Theor. Biol. **26**, 21 (1970).
29. E. Evans, Biophys. J. **14**, 923 (1974).
30. J. Ambjørn, B. Durhuus, J. Frölich, Nucl. Phys. B **257**, 433 (1985).
31. F. David, Phys. Lett. B **159**, 303 (1985).
32. V.A. Kazakov, K. Kostov, A.A. Migdahl, Phys. Lett. B **157**, 295 (1985).
33. M. Nielsen, L. Miao, J.H. Ipsen, O.G. Mouritsen, M.J. Zuckermann, Phys. Rev. E **54**, 6889 (1996).
34. D. Nelson, T. Piran, S. Weinberg (Editors), *Statistical Mechanics of Membranes and Surfaces*, 2nd edition (World Scientific, Singapore, 2003).
35. N. Ramakrishnan, P.B. Sunil Kumar, J.H. Ipsen, Phys. Rev. E **81**, 041922 (2010).
36. M. Meyer, M. Desbrun, P. Schröder, A.H. Barr, Vis. Math. **3**, 34 (2004).
37. A.I. Bobenko, B.A. Springborn, Discrete Comput. Geom. **38**, 740 (2007).
38. J. Lee, Phys. Rev. **71**, 211 (1993).
39. F. David, S. Leibler, J. Phys. II **1**, 959 (1991).
40. P. Pincus, Macromoleculs **9**, 386 (1976).
41. Y. Kantor, M. Kardar, D.R. Nelson, Phys. Rev. A **35**, 3056 (1987).
42. J. Banavar, A. Maritan, A.L. Stella, Science **252**, 825 (1991).
43. O. Farago, Y. Kantor, Phys. Rev. E **3**, 253 (2000).
44. F.H. Stillinger jr., Z.W. Salsburg, R.L. Kornegay, J. Chem. Phys. **43**, 932 (1965).
45. F. David, E. Guitter, Europhys. Lett. **3**, 1169 (1987).
46. F. David, E. Guitter, Nucl. Phys. B **295**, 332 (1988).